Essentiality of conserved amino acid residues in β-lactamase

Chikunova, A.

Chapter 6
Crystal structures of single-point mutants of BlaC

Based on the research articles:

Ilona van Alen, Aleksandra Chikunova, Adil A Safeer, Misbha Ud Din Ahmad, Anastassis Perrakis, Marcellus Ubbink (2021). The G132S Mutation Enhances the Resistance of Mycobacterium tuberculosis β-Lactamase against Sulbactam, *Biochemistry*. 60(28): 2236-2245

Wouter Elings, Aleksandra Chikunova, Danny B van Zanten, Ralphe Drenth, Misbha Ud Din Ahmad, Anneloes J Blok, Monika Timmer, Anastassis Perrakis, Marcellus Ubbink (2021). Two β-Lactamase Variants with Reduced Clavulanic Acid Inhibition Display Different Millisecond Dynamics, *Antimicrob Agents Chemother.* 65(8): e0262820

Abstract

Laboratory evolution studies on BlaC showed that reduced sensitivity to the inhibitors sulbactam and clavulanic acid can be caused by single amino acid substitutions. To understand the structural nature of the changes, several BlaC variants with reduced sensitivity for sulbactam or clavulanate were crystallized and their structures analyzed. Decreased sensitivity to sulbactam can be reached by stabilizing interactions, as shown for mutant D172N, or rearrangements in the active site, as demonstrated by BlaC G132S in complex with the adduct of sulbactam. The crystal structure of BlaC G132N, which displays reduced clavulanate sensitivity, showed a rearrangement near active site similar to BlaC G132S, with two conformations of active site residue Ser130 and formation of a cis-peptide bond in an active site loop.

Introduction

β-Lactamase inhibitors are used to overcome the resistance to β-lactam antibiotics caused by β-lactamases[242,243]. The first discovered inhibitor, clavulanic acid[244] (Figure 1.3), is structurally similar to penicillin and inhibits the enzyme via formation of a covalent complex that is hydrolyzed only very slowly. Another clinically approved inhibitor, sulbactam (Figures 1.3, 6.1), is a synthetic inhibitor that was developed in 1978 by Wayne E. Barth[245]. It is structurally similar to clavulanic acid and is currently used in the clinic in combination with either ampicillin or cefoperazone[79,243]. The adducts of clavulanate and sulbactam can exist in a *trans*-enamine form. It is this form that is hydrolyzed very slowly, inhibiting the enzyme (Figure 6.1) transiently, or alternatively, the imine adduct form can acylate an additional active site nucleophile, Ser130 to yield a cross-linked enzyme, which is irreversibly inactivated[246,247]. The enzyme-adduct complexes of BlaC were described with mass spectrometry[102,248] and x-ray crystallography[141]. Mass spectrometry on BlaC with clavulanate together with activity studies performed by Hugonnet and colleagues supported the conclusion that clavulanate inhibition is irreversible[102]. However, it was shown later that enzymatic activity recovers from inhibition with the half live for recovery of ~3 h, furthermore, the recovery can be accelerated by ions present in the buffer[248]. The recovery of enzymatic activity from sulbactam inhibition was observed already after 30 min[102].

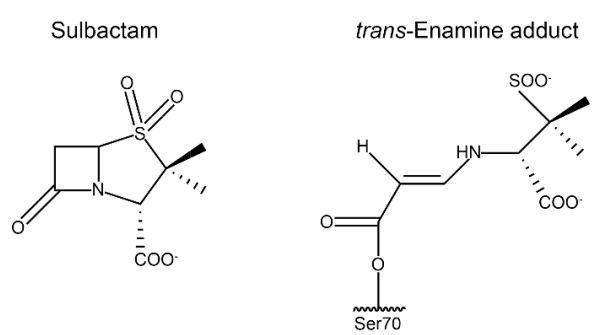

Figure 6.1. Structures of sulbactam and trans-enamine adduct of sulbactam covalently linked to Ser70.

One of the questions that was raised in the Ubbink research group was whether evolution against sulbactam inhibition through mutations in BlaC could easily occur. Decreased sensitivity could have a negative bearing on the effectiveness of combination therapy. For that purpose, a laboratory evolution experiment was carried out, yielding, among others, mutations A55E, G132S, and D172N mutants. BlaC A55E and D172N exhibited a slight decrease in sensitivity to sulbactam *in vivo*, but the activity of the purified enzymes was inhibited to the same degree as the wild type enzyme, suggesting changes in stability or

protein production *in vivo*[82]. Ala55 is located in a loop (Figure 6.2) and its Cα atom is 28 Å away from Cα of active site Ser70, which makes it unlikely that the mutation can affect enzyme activity, in line with the experimental findings. Asp172 is a part of an important structural element, the Ω-loop, but it is not conserved in class A β-lactamases, with alanine being the most abundant residue at this position (62% out of 494 class A β-lactamase sequences, see chapter 2 for details). BlaC D172N exhibits an increased melting temperature, in line with an increased stability that can explain the decreased sulbactam sensitivity *in vivo*[82]. Residue 132 is part of the one of the most conserved motifs in class A β-lactamase active sites – the Ser130-Asp131-Asn132 motif (SDN motif). Interestingly, BlaC harbors a glycine instead of an asparagine at position 132. BlaC G132S displayed reduced sensitivity for sulbactam, both *in vivo* and *in vitro* using an activity assay with nitrocefin as substrate. These findings indicate that G132 is involved in the interactions of sulbactam with the active site[82].

The substitution of Asn with Gly results in an enlarged active site in BlaC as compared to other β-lactamases. At the same time, the potential for stabilizing enzyme-substrate interactions via the Asn side chain is lost. The glycine at position 132 in BlaC could be one of the reasons for its broadened substrate specificity, paired with somewhat decreased overall activity compared to other class A β-lactamases. It has been proposed that substituents at the R^6 position (rest chain at β-lactam ring) of carbapenem (Figure 1.3) could be accommodated by this substitution[249]. For this reason, the reverse mutant G132N in BlaC was studied extensively. Soroka *et al.* showed that the G132N mutation increases the hydrolysis rate of nitrocefin, imipenem and aztreonam, while decreasing the hydrolysis rate of cephalosporins[84,85]. It also increases the resistance of the enzyme to clavulanic acid, but at the same time increases sensitivity to another inhibitor, avibactam (Figure 1.3)[84]. Elings *et al.* recently showed that BlaC G132N exists in two almost equally populated states in solution. Moreover, binding to the inhibitor influences the dynamic behavior of the enzyme, increasing the millisecond time scale chemical exchange in the active site[83].

To elucidate the relation between the inhibitor resistance and structural changes, the BlaC variants A55E, D172N, G132S, and G132N were crystallized, and the obtained x-ray diffraction structures were analyzed. Also, the structure of another variant, BlaC P226G, of the third-shell conserved residues discussed in chapter 2, was solved. Most structures show only subtle effects of the mutations. In the G132 variants the effects are more significant. An active site serine was found to occupy multiple orientations in G132 mutants, and an alternative conformation was found for one of the active site loops. The structures of BlaC G132S mutants were also solved with the adduct of sulbactam, which revealed a possible mechanism of inhibitor resistance.

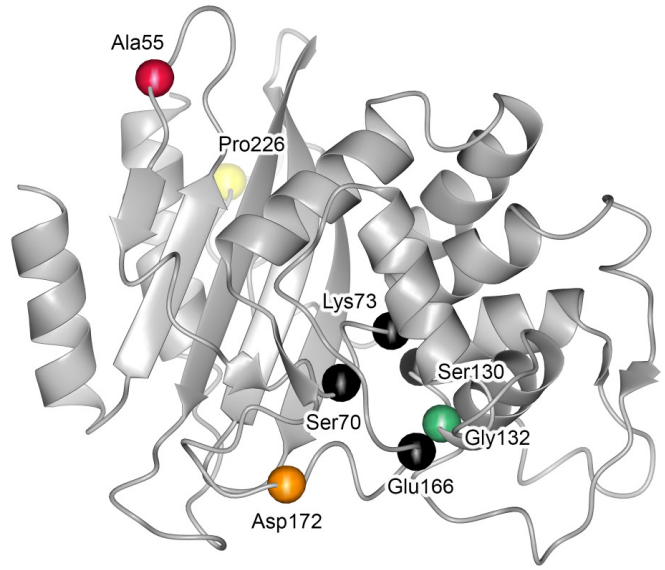

Figure 6.2. BlaC structure (2GDN[101]) with Cα atoms shown as spheres for active site residues (black) and for residues for which substitutions are discussed in this chapter (colors).

Results

To complement the findings about *in vivo* and *in vitro* activity of the variants of BlaC, the three-dimensional structures were determined using x-ray diffraction of crystals. The mutant proteins were produced in *Escherichia coli*, purified to homogeneity and crystallized as described in Material and Methods section. BlaC A55E, G132S and D172N were produced by Ilona van Alen, BlaC G132N was produced by Wouter Elings and Roeland de Wit and BlaC P226G was produced by Aleksandra Chikunova and Max Manley.

The phase problem was solved by molecular replacement with PDB entry 2GDN[249] as a model, except for the crystal soaked with inhibitor sulbactam, in which case entry 6H2K[141] was used. The structures had resolutions in the range of 1.6 – 1.3 Å and could be refined to high quality factors (Table 6.3). The overall structures of the variants were found to be very similar to that of wild type BlaC with average Cα RMSDs for A55E, D172N, P226G, G132N, G132S and G132S with sulbactam of 0.28, 0.32, 0.34, 0.33, 0.33 and 0.36 Å, respectively. Figure 6.2 presents overlays of the structures with that of wild type BlaC.

In BlaC A55E, the δ-carboxy group of Glu55 adds an extra negative charge on the surface of the protein. In the crystal lattice, the δ-carboxyl of Glu55 engages in a hydrogen bond with the symmetry-related side chain of Arg277 (Figure 6.4a). Notably, the lattice of the A55E mutant deviates from the commonly observed primitive orthorhombic lattice observed for other structures, crystallizing in the closely related primitive monoclinic lattice, presumably largely because of this mutated side chain and the new salt bridge. The δ-carboxy group also makes two hydrogen bonds involving water molecules.

The changes for D172N are less obvious, as the side chain of Asn172 occupies the same space as the aspartic acid in the wild type protein. The carboxamide group of Asn172 forms two highly favorable hydrogen bonding interactions with the side chain carboxyl of Asp179 and the carbonyl of the peptide bond between residues 178 and 179 (Figure 6.4b). These favorable interactions, which are not observed for wild type BlaC, stabilize the loop of residues 171–180 and are likely the cause of the increased thermostability of the D172N mutant.

BlaC P226G displays virtually no differences in comparison with the structure of wild type BlaC. Surprisingly, even the loop containing residue 226 displayed no changes (Figure 6.4c). An absence of the pyrrolidine ring, however, allowed for an additional ordered water to be present in a mutant structure.

In BlaC G132N the Asn side chain that is introduced at position 132 occupies the canonical position for class A β-lactamases (Figure 6.5a). The oxygen of the side chain is hydrogen

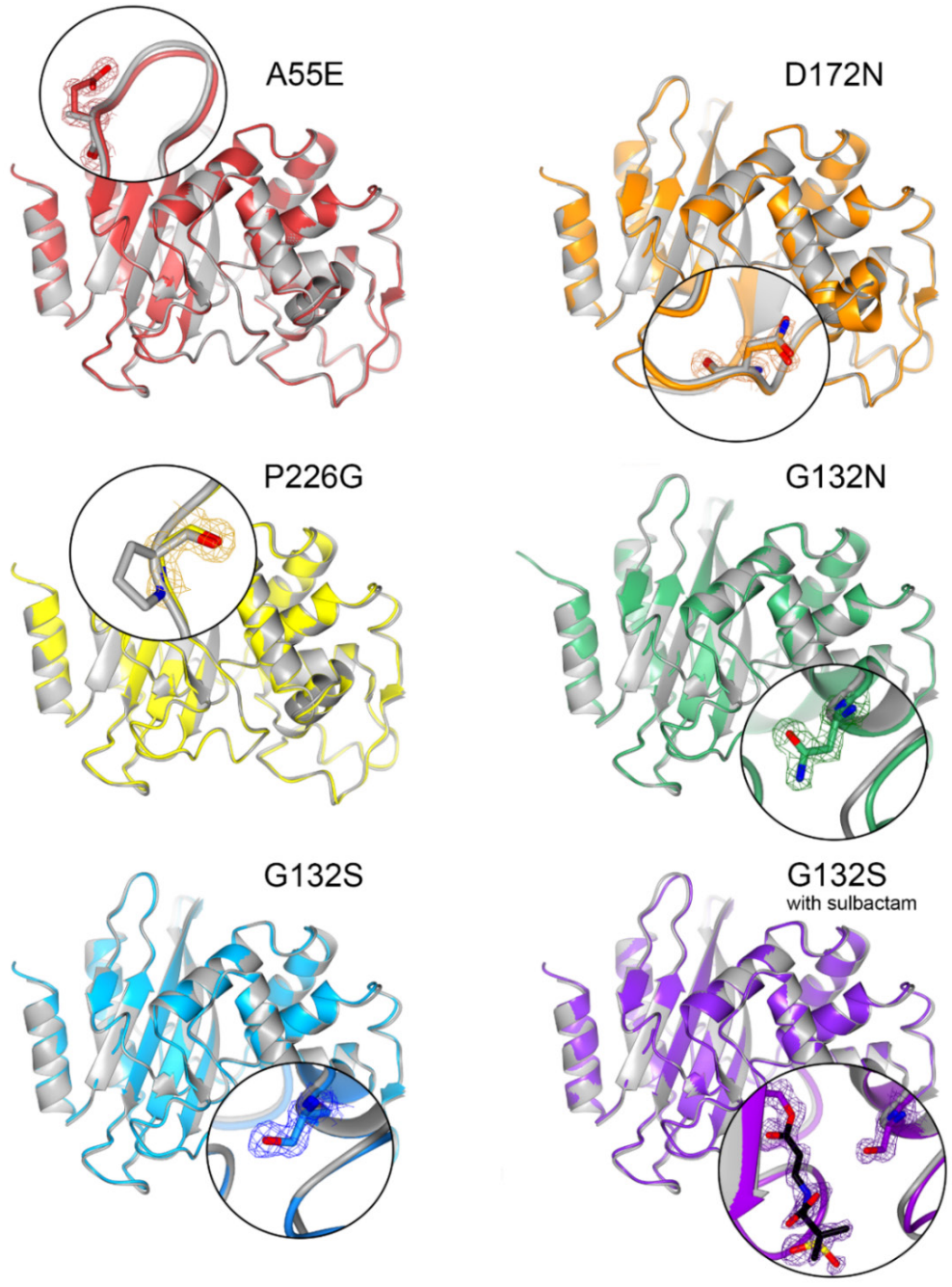

Figure 6.3. Overlay of wild type BlaC structure (2GDN[101], in grey) and mutants (in colors). Mutation sites are shown as close-ups in circles and mutated residues are shown in sticks. The $2mF_0$-DF_c electron density maps are shown in chicken wires with contour levels of 1 σ and extent radius of 5 Å. The electron density maps are pinned around mutated residues. The sulbactam adduct is shown in black sticks bound to the active site Ser70 (in purple sticks).

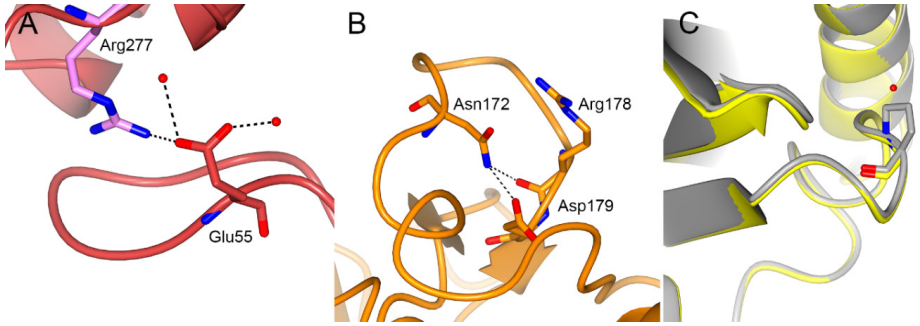

Figure 6.4. (A) Mutated residue Glu55 (in red) has an ionic interaction with symmetry-related Arg277 (in pink) and waters (red spheres); (B) Interactions of the side chain of Asn172; (C) Overlay of wild type BlaC (2GDN[101], in grey) and BlaC P226G (7A6Z, in yellow).

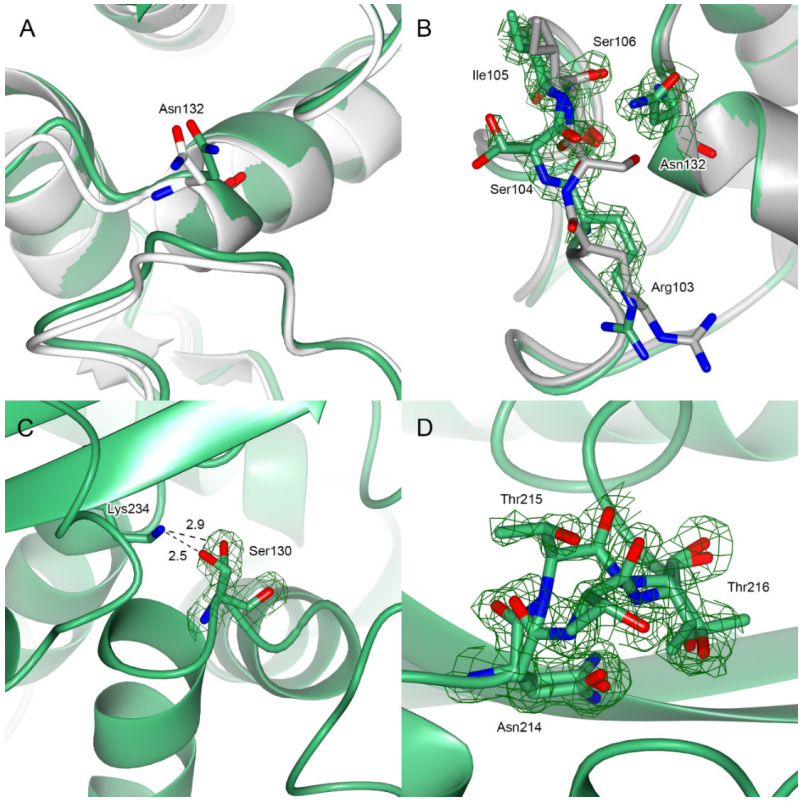

Figure 6.5. Structure of G132N mutant (7A74, in green) overlaid with TEM-76 (1YT4[234], in white) or wild type BlaC (2GDN[101], in grey). The 2mF0-DFc electron density map is centered on the selected residues and is shown in green chicken wire, with contour level 1 σ and extent radius 5 Å. (A) Side chain of the residue Asn132 in BlaC G132N occupies a position canonical in class A β-lactamases; (B)In BlaC G132N, the side chain of residue Ser104 flips to the surface, where it can be modeled in two alternative conformations, forcing the peptide bond with Ile105 into a cis conformation; (C) Residue Ser130 in BlaC G132N exists in two conformations; (D) Region 214-216 exists in multiple conformations.

bonded (2.7 Å) with the amine of Lys73. Strikingly though, the nitrogen of the Asn132 side chain hydrogen bonds (2.8 Å) to the carbonyl oxygen of residue Ser104. This interaction flips the side chain of Ser104 from the inside to the outside of the protein, where it adopts two conformations. This conformation in turn flips the carbonyl of Ser104 and forces the peptide bond with residue 105 to a cis conformation. This is notable as this is the only cis peptide conformation in this position in all 94 homologous structures in the PDB, as revealed by the LAHMA server[250]. This change propagates to residues 102-105, which adopt conformations distinct from the wild type BlaC (Figure 6.5b).

An interesting double conformation is also observed for the side chain of Ser130 (Figure 6.5c). In the structure of BlaC G132N this side chain occupies the position that is observed in all but six homologues in the PDB, making hydrogen bonds to the active site Lys234 amine (2.9 Å). In the second conformation the hydrogen bond is maintained, with the bond to the Lys234 amine becoming shorter (2.5 Å). Multiple conformations are also supported by the electron density for the Asn214, Thr215 and Thr216 loop region, two of which were modelled (Figure 6.5d). In this case, the occupancy of each modeled conformation is not equal and current modeling can only be considered an estimate indicative of the conformational dynamics.

In the G132S mutant, the side chain moiety of Ser104 is forced away by the side chain of Ser132 (Figure 6.6a) in the same manner that is observed in G132N mutant. The side chain of Ser104 is turned toward the protein surface, and the carbonyl oxygen of its peptide bond with Ile105 engages in a hydrogen bond with the newly introduced hydroxyl group of Ser132. This hydrogen bond again causes the peptide bond between residues 104 and 105 to assume a cis conformation. Two conformers are observed for Ser130 also in this structure (Figure 6.6b).

In the structure of the mutant with the trans-enamine adduct of sulbactam, the different positioning of the residues mediated by the G132S mutation as compared to that in wild-type BlaC is maintained, allowing the hydroxyl of Ser104 to form a hydrogen bond with one of the oxygens of the sulbactam sulfonyl moiety, not observed in the adduct with wild type BlaC (PDB entry 6H2K[141], Figure 6.6c). The interaction of the sulfonyl moiety with Arg171, observed in the latter structure, is also found in the BlaC G132S–adduct complex. This interaction reduces the rotational freedom of the sulfonyl group in the wild type enzyme to a single conformation. The side chain of Ile105 in the structure of the BlaC G132S–adduct complex is not flipped to the side of the active site entrance, as observed for the wild type BlaC–adduct complex and is likely pushing away the dimethyl group of the sulbactam adduct. Overall, the trans-enamine adduct of sulbactam has more interaction and better packing in BlaC G132S than in wild type BlaC (Figure 6.6d), which is in apparent contrast with the weakened inhibitory effect in the hydrolysis of substrates.

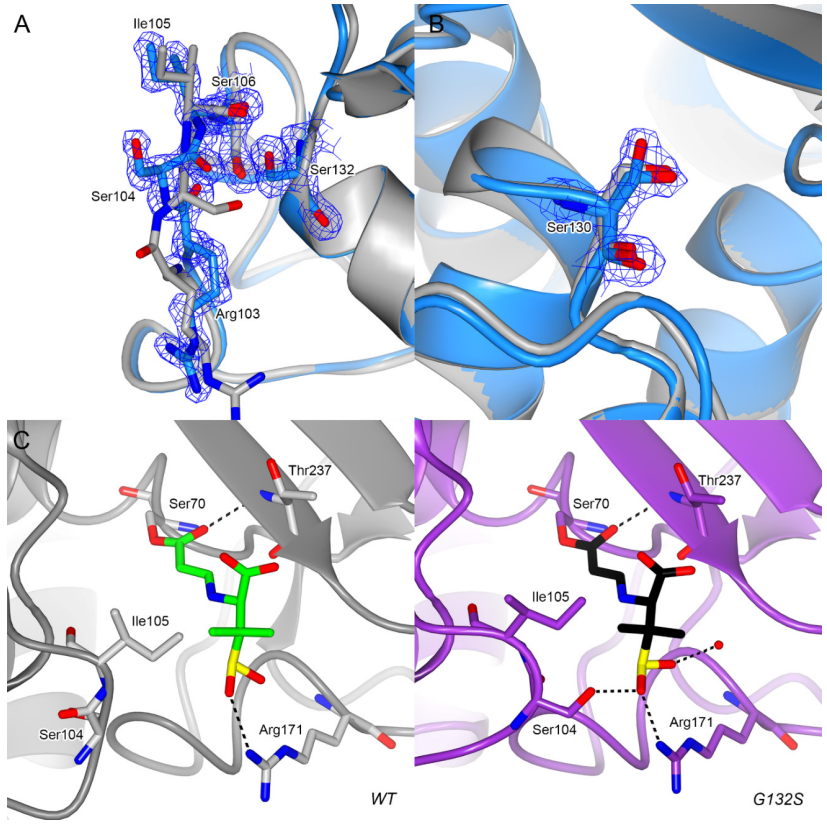

Figure 6.6. Structures of BlaC G132S. (A, B) Overlay of wild type BlaC (2GDN[101], in grey) and BlaC G132S (7A71, in azure). Residues 103-106 (A) and Ser130 (B) are shown in sticks. The side chain of Ser104 flips to the surface, forcing the peptide bond with Ile105 to a cis conformation. Residue Ser130 in the mutant structure exists in two conformations with almost equal occupation. The $2mF_0$-DF_c electron density map is centered on these residues and is shown in blue chicken wire, with contour level 1 σ and extent radius 5 Å; (C) Structure of the covalent trans-enamine adduct (in green or black) formed between sulbactam and wild type BlaC (in grey) (6H2K[141], left) and BlaC G132S (7A72, in purple, right). More interactions are involved in stabilization of the adduct in the mutant than in the wild type enzyme, with a hydrogen bond donated by Ser104 in its new orientation.

Discussion

In this chapter the structures of several single mutants of BlaC are discussed. Two variants, A55E and D172N, found in laboratory evolution with sulbactam activity as a selection pressure[82], displayed no mechanistic resistance to sulbactam, because they performed better than wild type enzyme against this inhibitor *in vivo*, but not *in vitro*. There can be a number of reasons for this, for example, higher activity against ampicillin, the antibiotic that was used in combination with sulbactam, or differences in the amount of active protein between the mutants, caused by differences in mRNA stability, translation, or folding, stability, or translocation of the protein. The increased stability is likely to be the reason for D172N mutant, as it was shown that this variant has a higher melting temperature than wild type enzyme[82]. The crystal structure presents a structural underpinning for increased stability of the ω-loop caused by interactions of Asn172 with residues 178 and 179. The interaction between Asn172 and Asp179 has a stabilizing effect similar to the Asp172-Asn179 interaction in D179N mutant discussed in chapter 5. Two negatively charged side chains at short distance destabilize the enzyme by repulsion. Therefore, given the short distance between Asp172 and Asp179 side chains in wild type BlaC, a hydrogen must be shared between the two carboxy groups. At near-neutral pH, replacement of one of the carboxy group (Asp) with a carboxyamide (Asn) is expected to yield a more stable structure.

The mechanism of somewhat higher sulbactam resistance for A55E mutant is less obvious. The additional surface charge may contribute to a higher solubility of BlaC and thus a somewhat higher concentration of active enzyme in the periplasmic state, but this hypothesis was not tested.

A change in a conserved amino acid is expected to yield considerable effects on the structure or function of the enzyme. However, as demonstrated by P226G mutant that is not always the case. This mutant displayed marginally lower activity *in vivo* yet has biophysical properties comparable to wild type enzyme *in vitro* (Table S2.2, Table S6.1), with somewhat higher activity displayed *in vitro* but not *in vivo*. The NMR spectrum of this mutant shows changes that are limited to the region around the site of the mutation (Figure S6.1) and the crystal structure is near-identical to that of the wild type enzyme. Therefore, the high conservation of this residue cannot be explained by its importance for the traits examined within this work. It is, however, plausible that highly conserved prolines located in the loops contribute to dynamics. Stacking interaction between conserved residues Pro226–Trp229–Pro252 was proposed to be important for modulating the H10 helix mobility in TEM-1[132].

For BlaC G132N, it was shown with NMR relaxation experiments that the substitution affects the dynamics in the active site in millisecond timescale[83]. The crystal structure also suggests

an increase in flexibility because several residues occur in more than one conformer. The relative occupancies of the Ser104 and Ser130 conformations observed in the crystal structure match those of the states observed in the NMR experiments. Moreover, these residues are positioned right in the region of the protein where broadening and exchange were observed with NMR spectroscopy. The x-ray and NMR observations may thus represent the same phenomenon. In this case, the two conformations, which are slowly exchanging at room temperature, were captured by flash freezing of the crystal prior to x-ray analysis. The region in which the effects of conformational exchange are observed with NMR is relatively large for single side chain movements, and the exchange is relatively slow (~80 s^{-1})[83]. As discussed in chapter 2, mutation in and around the active site affects the chemical shifts of many amide groups around the active site, which is explained by assuming that there is a network of interactions through hydrogen bonding and other electrostatic interactions, also involving many water molecules.

In the resting state structure of BlaC G132S, the side chain of Ile105 has moved 1.6 Å relative to its position in the structure of wild type BlaC, partly blocking the active site. This change is brought about by the backbone rearrangement due to the introduction of the Ser at position 132. Upon formation of the adduct of sulbactam, Ile105 keeps its position, whereas in the wild type enzyme, it rotates away. Interestingly, the backbone rearrangement in BlaC G132S leads to better interactions with the adduct, including a hydrogen bond from Ser104 to the sulfonyl group. This observation seems to be in contrast with the weakened inhibition by sulbactam observed by van Alen *et al.*[82]. However, the structure of sulbactam is very different from that of the adduct. The latter is an elongated molecule without rings, whereas sulbactam has two ring structures, which place the sulfonyl group in a different position in the active site. The reduced inhibitory effect of sulbactam can be explained by decreased access to Ser70, caused by the rearrangement of the loop containing Ser104 and Ile105.

The change in the position of the loop and the cis peptide bond configuration are induced by the newly introduced side chain at position 132 for both G132N and G132S, because the introduced side chain would cause steric collisions, were Ser104 to take the same position as in wild type BlaC. The two conformers of Ser130 observed in both G132S and G132N structure are reminiscent of observations in clavulanic acid-resistant variants of SHV, PSE-4 and CTX-M-14 β-lactamases. There, MD simulations[121] and x-ray crystallography[120,122,251] have shown that the presence of Arg234 rather than Lys234 causes a displacement of the Ser130 side chain, moving it further away from the reactive Ser70. This may prevent cross-linking between Ser70 and Ser130, which could explain the increased resistance of the enzyme to clavulanic acid.

Materials and Methods

Protein expression and purification

Protein was produced using *E. coli* BL21 (DE3) pLysS cells transformed with pET28a plasmids containing the *blaC* gene with an N-terminal His tag and TEV cleavage site. Protein was produced and purified as described in chapter 3 of this work and in van Alen *et al.* and Elings *et al.*[82,83]. PA-gel electrophoresis was used to evaluate the purity of the samples before samples were used for crystallization. Proteins were concentrated using Pierce™ (Thermo Scientific™) concentrators with cutoff 10 kDa.

Crystallization

Crystallization conditions for BlaC mutants were screened by sitting-drop vapor diffusion using the BCS, Morpheus, JCSG+ and PACT premier (Molecular Dimensions) screens at 20 ˚C with 100 nL drops with 1:1 ratio. The plates were pipetted by the NT8 Drop Setter (Formulatrix). Protein solutions were used with a concentration of 9 mg mL^{-1} for A55E, G132S, and D172N in 20 mM Tris buffer with 100 mM sodium chloride (pH 7.5) and 10 mg mL^{-1} for P226G mutant in 100 mM sodium phosphate buffer (pH 6.4). BlaC G132N was used at a concentration of 18 mg mL^{-1} in 100 mM MES/NaOH buffer, pH 6.4. To obtain crystals, it was necessary to supplement the protein with 100 mM sodium phosphate buffer and cross-seed with crystals from another BlaC mutant (G132S). Crystals for all mutants grew within two months under various conditions.

A selection of one to five crystals for each mutant were mounted on cryoloops in mother liquor with addition of up to 25% glycerol and vitrified in liquid nitrogen for data collection. In addition, four crystals of G132S BlaC were soaked in corresponding mother liquor with 10 mM sulbactam for 40 min. The conditions yielding crystals that were used for structure determination can be found in Table 6.1.

Table 6.1. Crystallization conditions

BlaC mutant	Crystallization condition
A55E	0.8 M disodium succinate
G132S	Sodium cacodylate (pH 6.5), 0.2 M sodium chloride, 2 M ammonium sulfate
G132S with sulbactam	0.1 M sodium cacodylate (pH 5.3), 15% PEG-SB, 10% ethylene glycol, 5% TMate
G132N	0.1 M Morpheus buffer 1 (pH 6.5), 30% EDO_8K, 0.09M halogens
D172N	0.1 M Morpheus buffer 1 (pH 6.5), 30% EDO_8K, 0.09M halogens
P226G	0.2 M Sodium malonate dibasic monohydrate, 20% PEG 3350

X-ray data collection, processing, and structure solution

X-ray diffraction data were obtained from a single crystal at the Swiss Light Source (SLS, Paul Scherrer Institute, Switzerland) for the A55E, G132S, D172N and P226G mutants and at the Diamond Light Source (DLS, Oxford, England) for BlaC G132N and G132S with sulbactam. Diffraction data were recorded on a Pilatus detector for G132N and G132S with sulbactam and on an Eiger detector for the other samples. The diffraction data extended to a resolution of 1.4 Å for A55E, G132S, and D172N and to 1.3 Å for G132S with sulbactam and P226G. The crystallographic diffraction data for G132N were recorded to resolution of 1.18 Å. The resolution was set to 1.55 Å based on $|I/\sigma I|$ and $CC_{1/2}$ values. Data were processed and integrated with XDS[226] and scaled with AIMLESS[227]. The structure was solved by molecular replacement using MOLREP[228] from the CCP4 suite[228] using PDB entry 2GDN[249] as a search model, except for G132S with sulbactam, in which case the wild type structure with sulbactam adduct was used (6H2K[141]). Building and refinement were performed using Coot and REFMAC[228]. The model was further optimized using the PDB-REDO webserver[230]. Structure validation showed a RamaZ score[231] of -0.09, 0.11, -0.09, 0.33, 0.36, and -0.20, for G132N, P226G, A55E, G132S, G132S with sulbactam and D172N respectively; 98-99% of all residues are within the Ramachandran plot favored regions with two outliers for all structures, namely, Cys69 and Arg220. According to MolProbity[229] the structure belongs to the 100th percentile for G132N and D172N, the 99th percentile for A55E and G132S with sulbactam, the 98th percentile for P226G and the 96th percentile for G132S. Data collection and refinement statistics can be found in Table 6.2. The following residues were modeled in two conformations: Arg128 and Ile186 for A55E; Ser130, Ile186, Asn197, Arg204, Lys219, Met264 and Glu283 for G132S; Arg39, Lys93, Met264 and Tyr272 for G132S with sulbactam; Arg128, Ser130 and Met264 for D172N; Lys93, Asp100, Ser104, Ser130, Val263 and Met264 for G132N; and Asp31, Glu35, Arg128, Ile186, Gln191, Arg204 and Met264 for P226G. For G132N, G132S and G132S with sulbactam, Ser104 was found in the cis conformation. In G132N structure residues N214-T215-T216 exist in multiple conformations and were modeled in two representative conformations.

In vivo activity studies

In vivo activity of P226G mutant was evaluated within the study described in Chapter 2 and later separately as described in Chapter 3.

Thermal stability

Thermal stability of P226G mutant was accessed as described in Chapter 3.

Kinetics

Kinetic parameters of the reaction of nitrocefin hydrolysis for P226G mutant were determined as described in Chapter 4.

NMR spectroscopy

NMR experiment for P226G mutant was performed as described in Chapter 3.

Table 6.2. Data collection and refinement statistics.

Data Collection	A55E	G132S	G132S +sulbactam	G132N	D172N	P226G
PDB ID	7A5T	7A71	7A72	7A74	7A5W	7A6Z
Beamline	X06SA (SLS)	X06SA (SLS)	I04-1 (DLS)	I04-1 (DLS)	X06SA (SLS)	X06SA (SLS)
Detector	EIGER X 16M	EIGER X 16M	PILATUS 6M-F	PILATUS 6M-F	EIGER X 16M	EIGER X 16M
Wavelength (Å)	1.000	1.000	0.912	0.912	1.000	1.000
Resolution (Å)	38.19-1.40 (1.42-1.40)	44.73-1.40 (1.42-1.40)	78.20-1.30 (1.32-1.30)	45.03-1.55 (1.58-1.55)	44.80-1.40 (1.42-1.40)	44.72-1.30 (1.32-1.30)
Space group	P 1 21 1	P 21 21 21	P 21 21 21	P 21 21 21	P 21 21 21	P 21 21 21
Unit cell a, b, c (Å)	39.00, 54.36, 53.69	53.30, 54.32, 78.85	53.49, 54.66, 78.20	54.00, 54.60, 79.40	54.03, 54.47, 78.78	53.52, 54.23, 79.05
$CC_{1/2}$	98.5 (75.2)	98.9 (65.4)	99.9 (65.5)	99.6 (54.6)	99.7 (77.7)	99.7 (77.0)
R_{pim} (%)	7.8 (34.4)	8.3 (69.8)	3.8 (58.2)	6.0 (52.6)	4.1 (52.4)	3.4 (39.3)
$\|I/\sigma I\|$	5.2 (1.7)	8.3 (2.6)	11.1 (1.3)	5.4 (1.1)	9.3 (1.8)	11.0 (1.6)
Completeness (%)	96.9 (94.2)	98.9 (97.4)	98.2 (99.8)	99.7 (99.0)	98.0 (98.0)	99.9 (99.9)
Multiplicity	2.5	3.7	5.7	1.8	3.0	6.5
Unique reflections	42718	45293	56098	34560	45377	57233
Refinement						
Atoms protein/ ligands/water	2013/59/207	2047/61/201	2034/37/221	2074/126/164	2008/29/156	2035/67/249
B-factors protein/ ligands/water ($Å^2$)	10/22/19	8/25/20	15/24/26	15/41/30	16/28/28	10/23/24
R_{work}/R_{free} (%)	14.8/17.7	13.0/16.1	15.2/18.9	13.4/18.2	13.5/17.2	13.1/15.1
Bond lengths RMSZ/ RMSD (Å)	1.056/ 0.014	1.270/ 0.016	1.249/ 0.016	1.016/ 0.017	1.236/ 0.016	1.475/ 0.018
Bond angles RMSZ/ RMSD (°)	1.085/ 1.781	1.120/ 1.837	1.168/ 1.940	1.070/ 2.010	1.155/ 1.919	1.148/ 1.873
Ramachandran plot preferred/outliers	248/2	248/2	259/2	245/2	245/2	249/2
RamaZ scores	-0.09	0.33	0.36	-0.09	-0.20	0.11
Clash score	2.42	4.52	1.94	7.10	1.48	1.84
MolProbity score	1.02	1.23	0.96	1.39	0.89	1.08

Supplementary materials

Table S6.1. In vivo and in vitro characteristics of wild type (WT) BlaC and the P226G variant. Kinetic parameters are given for nitrocefin hydrolysis in 100 mM sodium phosphate buffer (pH 6.4) at 25 °C. Melting temperature obtained with thermal shift assay method using hydrophobic dye.

Enzyme	k_{cat} ± SD[a] (s^{-1})	K_M ± SD[a] (μM)	k_{cat}/K_M[b] (x 10^5 $M^{-1}S^{-1}$)	MIC carbenicillin (μg mL^{-1})	Melting temperature[c] (°C)
WT	133 ± 7	281 ± 18	4.7 ± 0.5	1000	52 ± 0.5
P226G	248 ± 12	361 ± 34	6.9 ± 0.5	500	50 ± 0.5

[a] Standard deviation represents the deviation of three measurements;

[b] Errors represent the propagated standard deviation;

[c] Values represent average of triplicate measurement with technical error.

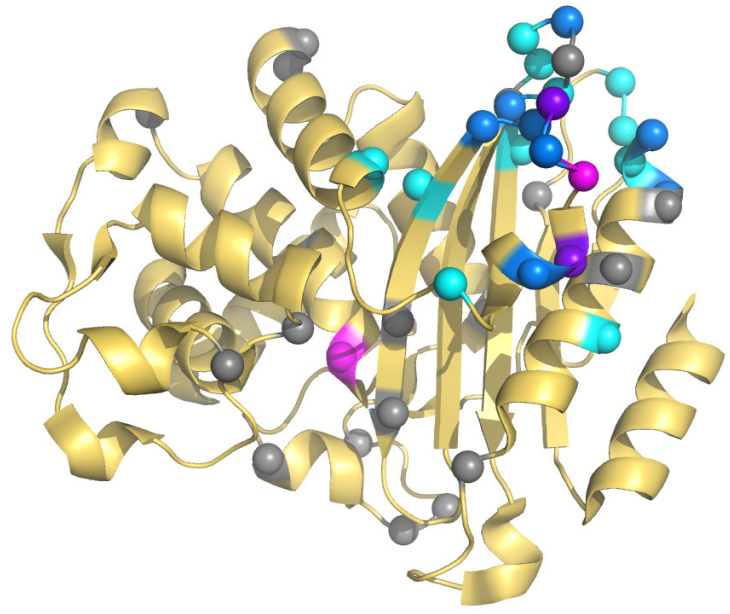

Figure S6.1. Average chemical shift differences (CSP) between the resonances of BlaC P226G and wild type BlaC mapped on structure (2GDN[101]). Residues are colored cyan for CSP > 0.025 ppm; blue for CSP > 0.05 ppm and purple for CSP > 0.1 ppm and grey for no data. Ser70 and Gly226 are shown in magenta. Relevant backbone nitrogen atoms are shown as spheres.